PCCP

ROYAL SOCIETY OF CHEMISTRY

PAPER

View Article Online
View Journal | View Issue

Cite this: *Phys. Chem. Chem. Phys.*, 2023, **25**, 6247

The catalytic hydrogenolysis of compounds derived from guaiacol on the Cu (111) surface: mechanisms from DFT studies

Destiny Konadu,[a] Caroline R. Kwawu,*[a] Elliot S. Menkah,[a] Richard Tia,[a] Evans Adei[a] and Nora de Leeuw[bc]

Received 18th September 2022,
Accepted 30th January 2023

DOI: 10.1039/d2cp04352a

rsc.li/pccp

Pyrolysis oils have inferior properties compared to liquid hydrocarbon fuels, owing to the presence of oxygenated compounds such as guaiacol, $C_6H_4(OH)(OCH_3)$. The catalytic hydro-deoxygenation (HDO) of phenolic compounds derived from guaiacol, *i.e.* catechol, phenol and anisole were investigated over the Cu (111) surface to unravel the elementary steps involved in the process of bio-oil upgrade. The phenolic compounds adsorb through their π systems to the surface, where steric effects of the methoxy group reduce the stability of anisole on the surface. To produce benzene, hydroxyl removal from catechol and phenol occurs in a stepwise fashion, where dehydroxylation of catechol is more challenging than phenol. Thermodynamically, catechol is the preferred oxygenated product, but it is the most challenging to transform to benzene, requiring an energy barrier of 1.8 eV to be overcome, which is similar to the HDO of anisole with an activation energy of 1.7 eV but more difficult than the HDO of phenol with an activation energy of 1.2 eV. The rate limiting steps in the HDO reactions are catechol dehydroxylation, anisole demethoxylation and phenol dehydroxylation. Our results show that *ortho* substituents impede C–O bond cleavage, as seen for catechol, whereas in the absence of an *ortho* substituent –OH cleavage is easier than $-OCH_3$ cleavage to form benzene.

1. Introduction

Fossil fuels serve as the primary fuel source for industrial and transportation activities in modern society, but they are non-renewable and reserves are being depleted.[1] Obtaining renewable liquid fuels from biomass is attractive, as this provides sustainable and reliable liquid fuels to use in our current transportation infra-structure. Recycling of waste wood biomass or lignocellulosic biomass is of particular interest, because these are non-edible sources which thus do not contribute to food insecurity or scarcity.[2]

Aside from biochemical processing, several thermochemical methods can be employed for the required depolymerisation of lignocellulosic biomass, such as pyrolysis, liquefaction and gasification.[3,4] Bio-oils obtained from fast pyrolysis have a high oxygen content, usually more than 10 wt% and even as much as 50 wt%,[5] which degrade its quality for transportation fuel purposes, namely causing low stability, low heating value, low pH, and high viscosity.[3,6,7] However, fast pyrolysis followed by catalytic upgrading through hydro-deoxygenation (HDO) is a particularly promising route for the removal of oxy-functional groups by molecular hydrogen in the presence of suitable catalysts.[8] Phenolic monomer compounds such as guaiacol, syringol, isoeuguenol, homovanillic acid, phenols, alkylphenols, anisole and catechol are abundant monomers in pyrolyzed bio-oil, in addition to dimers and oligomers. For example, pyrolytic lignin contains up to 30 wt% monomeric oxygenated compounds in the pyrolyzed bio-oil.[9] 2-Methoxy phenol (guaiacol) and 1,2-dihydroxybenzene (catechol) constitute major by-products from the thermal decomposition of biomass,[10–12] especially from the polyphenolic constituents such as lignin.[13]

Experimentally, HDO of phenolic compounds has been studied mainly on supported noble and non-noble metals, as well as over sulphide-based catalysts.[14–23] Using phenol, guaiacol and other types of substituted phenols,[8,9,24] a few studies have addressed HDO *via* a theoretical approach, usually using calculations based on the density functional theory (DFT).[17,19,25–28] For example, guaiacol HDO has been studied over the Ru (0001), Pt (111) and Cu (111) surfaces,[15,29,30] whereas the dissociation of phenol to phenoxy has been investigated on Pt,[26] Rh,[26] Pd[25] and Fe[25] surfaces. Our previous DFT studies have shown that on the Cu (111) surface, guaiacol upgraded by one mole of $H_{2(g)}$ produces preferentially catechol

[a] *Department of Chemistry, Kwame Nkrumah University of Science and Technology, Kumasi, Ghana. E-mail: kwawucaroline@gmail.com*
[b] *Department of Chemistry, Cardiff University, Cardiff, CF1 3AT, UK*
[c] *School of Chemistry, University of Leeds, Cardiff, CF1 3AT, UK*

over anisole with reaction rates of the order of 99.6×10^{-23} s^{-1} and 1.95×10^{-23} s^{-1}, respectively, where catechol formation is 99 times favoured over anisole formation on the Cu (111) surface. The rate-limiting steps were observed to be the dissociation of $-CH_3$ and –OH, respectively.[30] In this work, we have studied the complete upgrade of these oxygenated compounds, *i.e.* catechol, anisole and phenol, into a hydrocarbon (benzene).

2. Computational details

We have employed spin polarised calculations based on the density functional theory (DFT) as implemented in the Quantum ESPRESSO package,[31] which performs fully self-consistent DFT calculations to solve the Kohn–Sham equations.[32] The Perdew Burke Ernzerhof (PBE) GGA exchange–correlation functional was employed[33] with a plane wave basis set. Energy cut-offs of 40 Ry (544 eV) were considered for all systems, with a corresponding charge density cut-off of 320 Ry (4354 eV). Monkhorst-Pack *k*-point grids of $(7 \times 7 \times 7)$ and $(1 \times 1 \times 1)$ were used to sample the Brillioun zones for the bulk and p (4×4) surface slab, respectively.[34] The effects of the Fermi surface were treated by the smearing technique of Fermi–Dirac, using a smearing parameter of 0.003 Ry. Grimme's D2 correction was implemented to allow for dispersion corrections. An energy convergence threshold-defining self-consistency of the electron density was set to 10^{-6} eV and a beta defining mixing factor for self-consistency of 0.2. The graphics of the atomic structures were prepared with the XCrysDen software.[31] For all surface descriptions, asymmetric slab models were employed of the p (4×4) supercell of copper, comprising 64 copper atoms. The top three Cu layers of each slab were relaxed explicitly, while the Cu atoms in the bottom three layers were kept fixed at their bulk optimised positions to mimic the bulk material. All gas-phase molecules were optimized in a $10 \times 10 \times 10$ Å unit cell. Periodic boundary conditions were applied such that the central supercell is reproduced periodically throughout space.[34] A vacuum region of 20 Å was introduced between the surface slabs to avoid interactions between slabs and adsorbates in the *z*-direction. Transition states were searched using the climbing image nudged elastic band method (CI-NEB) as implemented in Quantum-Espresso. The CI-NEB was implemented by interpolating three images between the initial and final states and optimizing the images along the reaction coordinate. Each transition state was confirmed to have a single imaginary vibrational frequency.

The reaction energies were calculated relative to the reactant molecule:

$$\Delta E_{rxn} = \Delta E_{(p)} - \Delta E_{(r)} \quad (1)$$

where $E_{(p)}$ is the energy of the intermediate formed and $E_{(r)}$ is the energy of the reactants.

The relative activation barrier was obtained by using the equation:

$$\Delta E_a = E_{(TS)} - E_{(IS)} \quad (2)$$

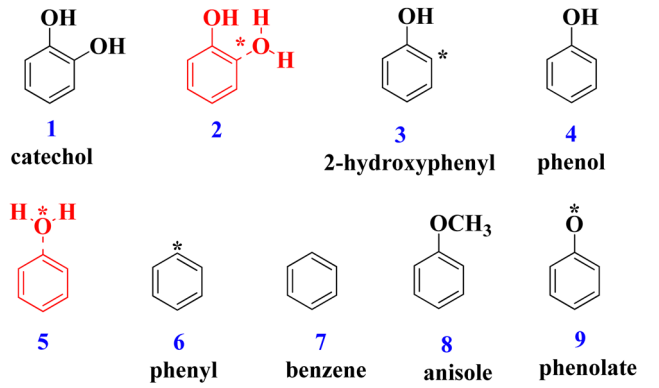

Fig. 1 Key reactants and intermediates considered in benzene formation on Cu (111). An asterisk indicates binding of a (mono- or di-) radical site to the metal surface.

where $E_{(TS)}$ is the energy of the transition state and $E_{(IS)}$ is the energy of the intermediate from which the transition state is formed.

In this study, enthalpy changes were calculated rather than free energy changes. As is common in these types of calculations, zero-point vibration energies and entropy contributions were not considered, which will not, however, impact the reaction energies significantly. All the adsorbates investigated on the Cu (111) surface are shown as structures **1** to **9** in Fig. 1. Where transition states are labelled, **1–2**, for example, denotes the transformation from adsorbate **1** to adsorbate **2**.

3. Results and discussion

Our earlier work[30] has shown that catechol is produced from guaiacol *via* direct demethylation into catecholate, followed by the concerted re-hydrogenation of catecholate into catechol. Anisole formation *via* the direct dehydroxylation of guaiacol followed by hydrogenation was found to be less favoured on Cu (111), both kinetically and thermodynamically. We observed that the C_{aryl}–OH cleavage into anisole is more challenging than the C_{akyl}–O bond cleavage into catechol, hence leading to the preferred formation of catechol over anisole.[30]

To better understand, and thus be able to control, the catalytic deoxygenation reaction of phenolics on Cu (111) into pure hydrocarbon end-products, *e.g.* benzene, we have studied the detailed surface reaction mechanisms involved in the upgrade of the oxygenated phenolic compounds formed from guaiacol. As seen in Fig. 2, the bond lengths of C_{ring}–OH and

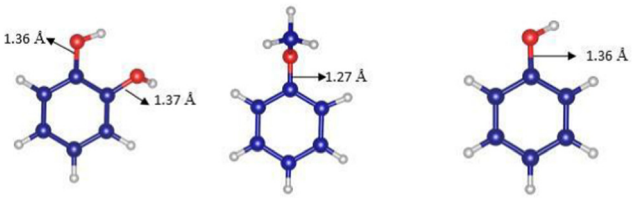

Fig. 2 Structural illustration and bond parameters of catechol, anisole and phenol in the gas phase. O: red; C: blue; H: white.

C_{ring}–OCH_3 are 1.36 Å and 1.27 Å, respectively. Hence, from the point of view of bond lengths, the C_{ring}–OH cleavage in catechol and phenol should be a similar process, whereas the C_{ring}–OCH_3 bond cleavage in anisole would be more difficult to achieve. However, bonds lengths can alter when the molecules are adsorbed at the Cu (111) surface.

Our calculations of the adsorption at the Cu (111) surface show that catechol, phenol, benzene and anisole all adsorb parallel to the surface *via* the benzene π system. There was no correlation between the binding energies and the binding strength as inferred from the Cu–C bond distances to the surfaces (see Table 1). Electron-donating groups activate the benzene ring for reaction by increasing the electron density on the π ring, as seen for –OH and $–OCH_3$, where the electron density of catechol will be highest, thereby making it the most reactive towards the surface. Although anisole has an attached electron-donating group, the bulky nature of the $–CH_3$ group and the parallel adsorption of the molecule makes its interaction to the surface weaker (see Fig. 3). The energies in Table 1 suggest that in a thermodynamically controlled reaction, the trend in yields observed would be catechol > phenol > benzene > anisole.

To understand the details of the benzene formation process, Scheme 1 is proposed and the possible pathways are investigated.

3.1 Catechol upgrade

Two routes were considered for the hydrogenolysis of catechol (structure 1) to benzene, either –OH removal *via* the direct deoxygenation (DDO) pathway or $–H_2O$ removal *via* the hydrogenation–dehydration (HD) route (Scheme 1). After dehydroxylation, the ring is further hydrogenated to produce phenol. Along the HD path, we first considered the formation of water *via* intermediate **2** (see Fig. 1). However, this path was not feasible because intermediate **2** did not form. Water is formed in a concerted fashion, where the hydrogen is abstracted from the neighbouring hydroxyl and water is formed as a leaving group, leading to the formation of the phenolate intermediate **9** (Fig. 1). Hence, catechol will transform through dehydroxylation to form phenolate, as shown in the red pathway in Fig. 4.

The kinetically accessible pathway for benzene formation from anisole is highlighted in blue and the path from catechol is highlighted in red. The activation energies and reaction energies are reported relative to the isolated reactants, *i.e.* catechol, hydrogen gas, and the Cu (111) surface, where zero-point vibrational energy (ZPVE) contributions were not considered. * on the adsorbate indicates the sites of decomposition and radical formation.

Table 1 Adsorption energies of catechol, phenol, benzene and anisole and their various shortest bonding distances of adsorbate atoms (C) to Cu (111) surface atoms

Aromatics	Adsorption energy/eV	(Cu–C)/Å
Catechol	−2.18	2.59
Phenol	−1.54	2.58
Benzene	−1.14	2.31
Anisole	−0.72	2.61

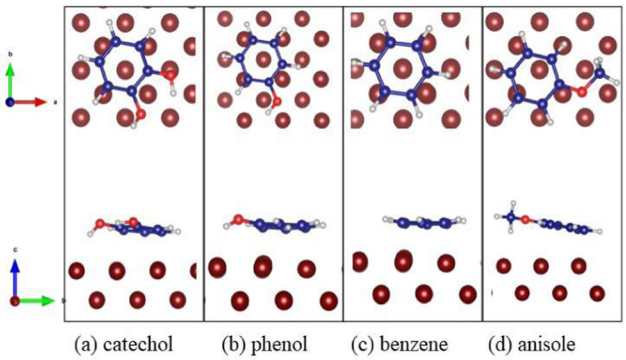

Fig. 3 Adsorption configurations of catechol (a), phenol (b), benzene (c) and anisole (d) on the Cu (111) surface. Cu: brown; O: red; C: blue; H: white.

From the energetics shown in the reaction profile in Fig. 4, phenol formation will proceed *via* the direct cleavage of the hydroxyl (–OH) group into phenolate. In turn, phenolate on protonation into phenol undergoes direct hydroxyl cleavage from phenol into phenyl, which is subsequently hydrogenated to benzene. In catechol, –OH cleavage needs to overcome an energy barrier of 1.78 eV to form phenolate, but hydrogenation to form phenol requires no energy barrier to be overcome. Dehydroxylation again leads to phenyl formation through a barrier of 1.2 eV. Hydrogenation of phenyl to form benzene is barrier-free.

3.2 Anisole upgrade

As shown in Scheme 1, anisole can be reduced *via* two possible paths, *i.e.* demethylation (DM) into phenolate (**9** in Fig. 1) or demethoxylation (DMO) to form phenyl. Phenolate can be protonated into phenol and subsequently transformed into phenyl (as seen in the catechol transformation pathway). Finally, the phenyl produced *via* DM and DMO can be hydrogenated into benzene.

In Fig. 4, it is seen that phenol formation from anisole requires a barrier of 1.7 eV to be overcome to lead to phenolate formation, followed by a barrier-less step to form phenol. However, benzene is formed from anisole following a different path, *i.e.* through demethoxylation over a barrier of 1.7 eV and subsequent barrier-less hydrogenation of phenyl into phenol. Demethoxylation and demethylation of anisole compete with barriers of 1.7 eV to form benzene and phenol, respectively, but due to the stability of phenol its transformation into benzene is not the most likely pathway.

3.3 Phenol upgrade

Demethylation of anisole is seen to be slightly more favourable (E_a = 1.7 eV) than the dehydroxylation from catechol (E_a = 1.8 eV) into phenol. This shows that although catechol formation is favoured on Cu (111) both kinetically and thermodynamically, catechol transformation into phenol and benzene is more challenging compared to anisole, due to the difficulty of removing –OH from catechol.

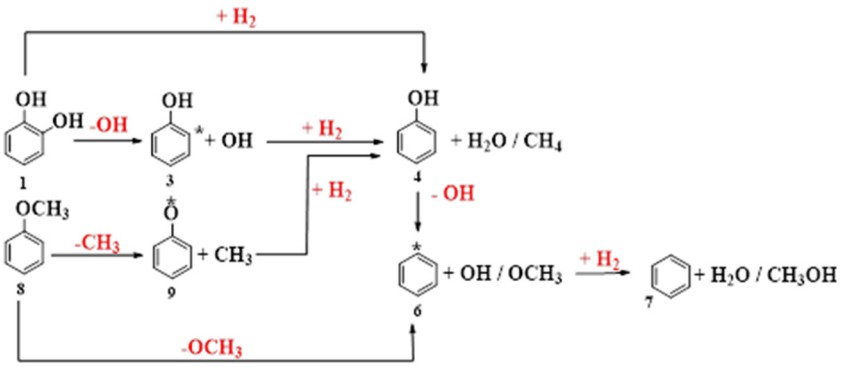

Scheme 1 Reaction network for the decomposition of catechol and anisole into phenol and benzene *via* HDO on Cu (111).

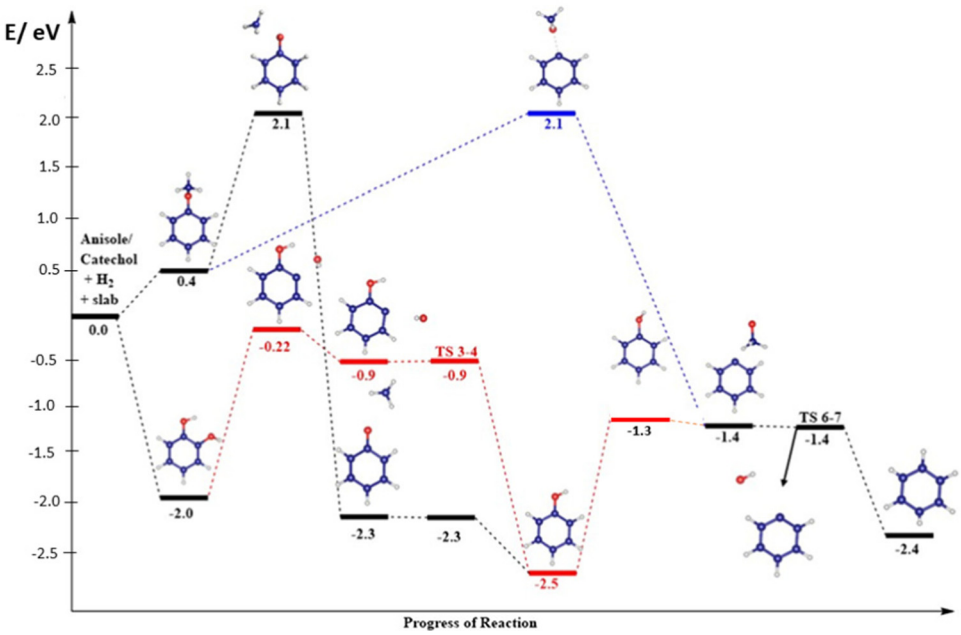

Fig. 4 The overall preferred path for the formation of benzene *via* the HDO reaction on Cu (111), showing the energies of the different species with respect to the surface and isolated adsorbates.

The energetics from our earlier work show that the rate-limiting steps for guaiacol transformation have energy barriers of 2.0 eV to form catechol and 2.1 eV to form anisole, with reaction rates of the order of 99.6×10^{-23} s^{-1} and 1.95×10^{-23} s^{-1}, respectively, where catechol formation is 99 times faster than anisole formation on the Cu (111) surface.[30]

There, we have shown that the rate-limiting steps in the formation of catechol from guaiacol, and subsequently phenol and benzene from guaiacol feedstock are the same, as the direct demethylation step into catecholate is the slowest step. The kinetic steps after catechol and anisole transformations are less than 2.0 eV, making the catechol and anisole formation the most challenging steps in the guaiacol upgrade. Thermodynamically, the products formed from guaiacol will be favoured in the order catechol > phenol > benzene > anisole, as shown in Table 1. These results show that conducting bio-oil upgrade at extreme temperatures for a long reaction time will form more catechol than phenol, benzene or anisole. Kinetically, however, the products from guaiacol will be favoured in the order catechol ~ phenol ~ benzene > anisole, but starting with an anisole feedstock, the formation of phenol and benzene is not selective kinetically, and equal proportions of phenol and benzene will be formed in a kinetically controlled reaction.

From Fig. 4, the phenol upgrade into benzene involves dehydroxylation with an energy barrier of 1.2 eV as the rate-limiting step. In general, kinetically phenol upgrade into benzene is favoured over anisole (E_a = 1.7 eV), which is also faster than the conversion of catechol into benzene (1.8 eV), and the transformation of guaiacol into benzene (2.0 eV).

These results show that upgrade of the *ortho*-substituted compounds like guaiacol and catechol is slower than the upgrade of anisole and phenol without *ortho*-substituents.

The –OH removal (E_a = 1.2 eV) is seen to be favoured kinetically over the –OCH_3 (1.7 eV) > –(OH)OH (1.8 eV) > –(OH)CH_3 (2.0 eV) > –(OCH_3)OH (2.1 eV) bond cleavages on the Cu (111) surface during hydrogenation.

4. Conclusion

We have used periodic DFT calculations to investigate the adsorption and hydro-deoxygenation of catechol, phenol and anisole on the Cu (111) surface. Catechol, phenol and anisole all adsorb in a flat position at an average distance of 2.59 Å from the copper surface. The adsorption energies decrease in the order of catechol > phenol > benzene > anisole, which should therefore be the trend in product yields in a thermodynamically controlled reaction. Neither catechol nor anisole converts selectively to phenol or benzene. The rate-limiting step for both anisole and catechol transformation into phenol and benzene is limited by the initial demethoxylation, demethylation and dehydroxylation of the anisole and catechol molecules. Thus, the Cu (111) surface needs to be more reactive towards C–O hydrogenolysis to improve the selectivity of the surface towards benzene production over phenol.

Code availability

Quantum Espresso is an opensource code available at **https://www.quantum-espresso.org/**.

Author contributions

Data were collected and the manuscript written by Mr Destiny Konadu. Research concept was developed by Dr Caroline Rosemyya Kwawu, Prof. Richard Tia and Prof. Nora de Leeuw. Work was supervised by Dr Caroline Rosemyya Kwawu, Prof. Evans Adei and Dr Elliot Menkah. Manuscript was revised by Dr Caroline Rosemyya Kwawu, Prof. Evans Adei and Prof. Nora de Leeuw.

Conflicts of interest

No conflicts of interest.

Acknowledgements

CRK is grateful for funding for The World Academy of Sciences (grant 18-032 RG/CHE/AF/AC_I). CRK and NHdL acknowledge the UK Royal Society and Leverhulme Trust for a research grant under the Royal Society-Leverhulme Africa Postdoctoral Fellowship Award Scheme (grant LAF\R1\180013). CRK is grateful for grants from The World Academy of Sciences (TWAS) and Swedish International Development Cooperation Agency (SIDA). CRK and NHdL thank the Royal Society UK and Leverhulme Trust for a research grant under the Royal Society-Leverhulme Africa Postdoctoral Fellowship Award Scheme. RT, EA and NHdL acknowledge the UK's Royal Society and Leverhulme Trust for a research grant under the Royal Society-Leverhulme Africa Award Scheme. The authors acknowledge the Center for High Performance Computing (CHPC), South Africa for additional computing resources.

References

1 R. A. Kerr, An oil gusher in the offi ng, but will it be enough?, *Science*, 2012, **338**(6111), 1139.
2 G. W. Huber, S. Iborra and A. Corma, Synthesis of transportation fuels from biomass: Chemistry, catalysts, and engineering, *Chem. Rev.*, 2006, **106**(9), 4044–4098.
3 R. French and S. Czernik, Catalytic pyrolysis of biomass for biofuels production, *Fuel Process. Technol.*, 2010, **91**(1), 25–32, DOI: **10.1016/j.fuproc.2009.08.011**.
4 W. Chen, Z. Luo, C. Yu, Y. Yang, G. Li and J. Zhang, Catalytic conversion of guaiacol in ethanol for bio-oil upgrading to stable oxygenated organics, *Fuel Process. Technol.*, 2014, **126**, 420–428, DOI: **10.1016/j.fuproc.2014.05.022**.
5 M. Saidi, F. Samimi, D. Karimipourfard, T. Nimmanwudipong, B. C. Gates and M. R. Rahimpour, Upgrading of lignin-derived bio-oils by catalytic hydrodeoxygenation, *Energy Environ. Sci.*, 2014, **7**(1), 103–129.
6 W. Mu, H. Ben, A. Ragauskas and Y. Deng, Lignin Pyrolysis Components and Upgrading-Technology Review, *Bioenergy Res.*, 2013, **6**(4), 1183–1204.
7 H. Wang, J. Male and Y. Wang, Recent advances in hydrotreating of pyrolysis bio-oil and its oxygen-containing model compounds, *ACS Catal.*, 2013, **3**(5), 1047–1070.
8 P. M. Mortensen, J. D. Grunwaldt, P. A. Jensen, K. G. Knudsen and A. D. Jensen, A review of catalytic upgrading of bio-oil to engine fuels, *Appl. Catal., A*, 2011, **407**, 1–19, DOI: **10.1016/j.apcata.2011.08.046**.
9 C. Zhao, Y. Kou, A. A. Lemonidou, X. Li and J. A. Lercher, Hydrodeoxygenation of bio-derived phenols to hydrocarbons using RANEY® Ni and Nafion/SiO2 catalysts, *Chem. Commun.*, 2010, **46**(3), 412–414.
10 Z. Maskos and B. Dellinger, Radicals from the oxidative pyrolysis of tobacco, *Energy Fuels*, 2008, **22**(3), 1675–1679.
11 Z. Maskos, L. Khachatryan and B. Dellinger, Precursors of radicals in tobacco smoke and the role of particulate matter in forming and stabilizing radicals, *Energy Fuels*, 2005, **19**(6), 2466–2473.
12 E. B. Ledesma, N. D. Marsh, A. K. Sandrowitz and M. J. Wornat, An experimental study on the thermal decomposition of catechol, *Proc. Combust. Inst.*, 2002, **29**(2), 2299–2306.
13 S. Chu, A. V. Subrahmanyam and G. W. Huber, The pyrolysis chemistry of a β-O-4 type oligomeric lignin model compound, *Green Chem.*, 2013, **15**(1), 125–136.
14 Z. He, X. Wang, E. Laurent and B. Delmon, Hydrodeoxygenation of model compounds and catalytic systems for pyrolysis bio-oils upgrading, *Catal. Sustainable Energy*, 2013, **1**(1), 28–52.
15 C. C. Chiu, A. Genest, A. Borgna and N. Rösch, Hydrodeoxygenation of guaiacol over Ru(0001): A DFT study, *ACS Catal.*, 2014, **4**(11), 4178–4188.

16 R. C. Runnebaum, T. Nimmanwudipong, D. E. Block and B. C. Gates, Catalytic conversion of compounds representative of lignin-derived bio-oils: A reaction network for guaiacol, anisole, 4-methylanisole, and cyclohexanone conversion catalysed by Pt/γ-Al2O3, *Catal.: Sci. Technol.*, 2012, **2**(1), 113–118.
17 T. Nimmanwudipong, C. Aydin, J. Lu, R. C. Runnebaum, K. C. Brodwater and N. D. Browning, *et al.*, Selective hydrodeoxygenation of guaiacol catalyzed by platinum supported on magnesium oxide, *Catal. Lett.*, 2012, **142**(10), 1190–1196.
18 H. Ben, G. A. Ferguson, W. Mu, Y. Pu, F. Huang and M. Jarvis, *et al.*, Hydrodeoxygenation by deuterium gas - A powerful way to provide insight into the reaction mechanisms, *Phys. Chem. Chem. Phys.*, 2013, **15**(44), 19138–19142.
19 H. Wan, R. V. Chaudhari and B. Subramaniam, Catalytic hydroprocessing of p-cresol: Metal, solvent and mass-transfer effects, *Top. Catal.*, 2012, **55**(3–4), 129–139.
20 S. Jin, W. Guan, C. W. Tsang, D. Y. S. Yan, C. Y. Chan and C. Liang, Enhanced Hydroconversion of Lignin-Derived Oxygen-Containing Compounds Over Bulk Nickel Catalysts Though Nb2O5 Modification, *Catal. Lett.*, 2017, **147**(8), 2215–2224.
21 H. Ohta, H. Kobayashi, K. Hara and A. Fukuoka, Hydrodeoxygenation of phenols as lignin models under acid-free conditions with carbon-supported platinum catalysts, *Chem. Commun.*, 2011, **47**(44), 12209–12211.
22 M. J. Girgis, B. C. Gates and M. J. Girgis, Reactivities, Reaction Networks, and Kinetics in High-Pressure Catalytic Hydroprocessing, *Ind. Eng. Chem. Res.*, 1991, **30**(9), 2021–2058.
23 H. Lesnard, M. L. Bocquet and N. Lorente, Dehydrogenation of aromatic molecules under a scanning tunneling microscope: Pathways and inelastic spectroscopy simulations, *J. Am. Chem. Soc.*, 2007, **129**(14), 4298–4305.
24 H. Xu, K. Wang, H. Zhang, L. Hao, J. Xu and Z. Liu, Ionic liquid modified montmorillonite-supported Ru nanoparticles: Highly efficient heterogeneous catalysts for the hydrodeoxygenation of phenolic compounds to cycloalkanes, *Catal.: Sci. Technol.*, 2014, **4**(8), 2658–2663.
25 A. J. R. Hensley, Y. Wang and J. S. McEwen, Phenol deoxygenation mechanisms on Fe(110) and Pd(111). ACS, *Catalysis*, 2015, **5**(2), 523–536.
26 M. L. Honkela, J. Björk and M. Persson, Computational study of the adsorption and dissociation of phenol on Pt and Rh surfaces, *Phys. Chem. Chem. Phys.*, 2012, **14**(16), 5849–5854.
27 C. A. Fisk, T. Morgan, Y. Ji, M. Crocker, C. Crofcheck and S. A. Lewis, Bio-oil upgrading over platinum catalysts using in situ generated hydrogen, *Appl. Catal., A*, 2009, **358**(2), 150–156.
28 P. Mäki-Arvela and D. Y. Murzin, Hydrodeoxygenation of Lignin-Derived Phenols: From Fundamental Studies towards Industrial Applications, *Catalysts*, 2017, **7**(9), 265.
29 J. Lu, S. Behtash, O. Mamun and A. Heyden, Theoretical Investigation of the Reaction Mechanism of the Guaiacol Hydrogenation over a Pt(111) Catalyst, *ACS Catal.*, 2015, **5**(4), 2423–2435.
30 D. Konadu, C. R. Kwawu, R. Tia, E. Adei and N. H. de Leeuw, Mechanism of guaiacol hydrodeoxygenation on cu (111): Insights from density functional theory studies, *Catalysts*, 2021, **11**(4), 523.
31 P. Giannozzi, S. Baroni, N. Bonini, M. Calandra, R. Car and C. Cavazzoni, *et al.*, QUANTUM ESPRESSO: A modular and open-source software project for quantum simulations of materials, *J. Phys.: Condens. Matter*, 2009, **21**(39), 20.
32 S. Grimme, J. Antony, S. Ehrlich and H. Krieg, A consistent and accurate ab initio parametrization of density functional dispersion correction (DFT-D) for the 94 elements H-Pu, *J. Chem. Phys.*, 2010, **132**, 154104.
33 J. P. Perdew, K. Burke and M. Ernzerhof, Generalized gradient approximation made simple, *Phys. Rev. Lett.*, 1996, **77**(18), 3865–3868.
34 J. D. Pack and H. J. Monkhorst, 'special points for Brillouin-zone integrations'-a reply, *Phys. Rev. B: Solid State*, 1977, **13**(4), 1748–1749.

